

1 ***Response to Editor Comments***

2 We thank the editor for the constructive suggestions/comments. Below we provide
3 a point-by-point response to individual comments (comments in italics, responses in
4 plain font; figures used in the response are labeled as Fig. R1, Fig. R2,...).

5

6 ***Comments and suggestions:***

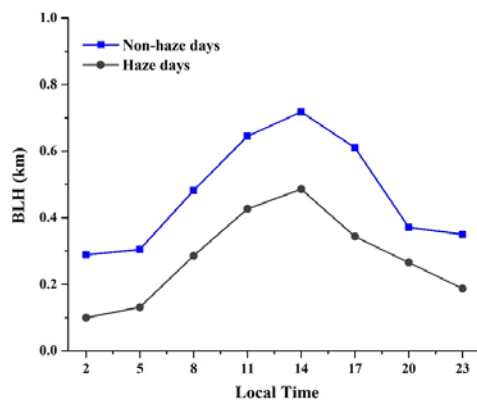
7 *You and your coauthors have addressed most of the referees' comments*
8 *satisfactorily. However, I remain concerned about your boundary layer depth estimates*
9 *based solely on MAX-DOAS data. Your analysis would be strengthened by independent*
10 *BL depth estimates based on, e.g., radiosonde data from locations not too distant from*
11 *Hefei. I believe that there are data available from Nanjing and Shanghai covering your*
12 *observation period. Although there are only 2 observations per day, they are at times*
13 *(at 0 and 12 UTC) that could yield some information about diurnal variability. This*
14 *manuscript on BL depth climatology in China that is also currently in review might be*
15 *worth looking at as well: <http://www.atmos-chem-phys-discuss.net/acp-2016-564/>.*

16 **Responses and Revisions:**

17 We accept your suggestions about boundary layer (BL) depth and we have
18 calculated BL height from ground meteorological observation data. As the Editor
19 pointed out, Radiosonde data is a good choice but there are only 2 observations per day
20 (at 8 and 20 Local time), so it might be difficult to explain the daytime variation of BL
21 height for the case study on 20 Nov, 2013 (see section 4.3). Fortunately, we have found
22 other meteorological data to calculate BL height in the revised ms. We used the national
23 standard method (GB/T13201-91, referred to as GB method) of China, to calculate the
24 height of atmospheric boundary layer. The GB method considers the thermal condition

25 of the surface layer greatly depends on the heating and cooling degrees of the ground.
26 In the revision, the entire year (from July 2013 to June 2014) of the surface
27 meteorological data acquired by the China Meteorological Administration (CMA) data
28 network was used to calculate the boundary layer height (BLK) in Hefei. Detailed
29 information about the GB method and calculation formula can be found in the
30 supplement. The calculated BL height is at a 3-hours resolution (at 2, 5, 8, 11, 14, 17, 20
31 and 23 Local time).

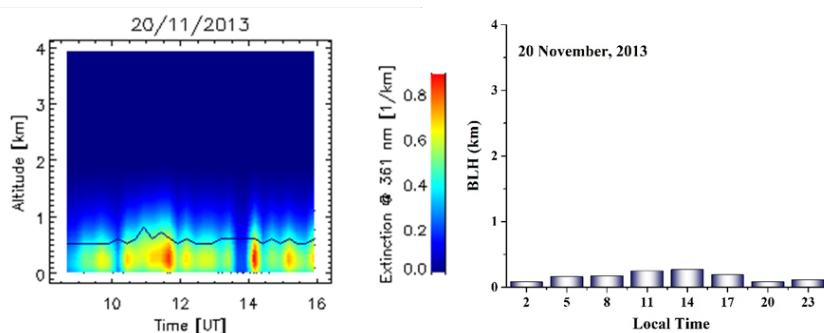
32 Diurnal variation of boundary layer height (BLK) on non-haze and haze days is
33 shown in Fig. R1. As we suggested in the original ms, BLH is indeed low in the
34 morning and night, and high during the daytime. These results further support our
35 original interpretation that the diurnal variation of GEM and PBM could be related to
36 changes in the height of urban boundary layer (section 4.2, second paragraph).



37
38 **Fig. R1.** Diurnal variation of boundary layer height (BLK) on non-haze and haze
39 days in Hefei. Notes: the atmospheric boundary layer height data were calculated by the
40 GB method.

41
42 Figure R2 (Figure S4 in the revised supplement) showed the boundary layer height
43 from the retrieved aerosol extinction profile (left). In order to strengthening boundary

44 layer height results, boundary layer height calculated from CMA meteorological
45 observation data in Hefei for 20 November, 2013 was shown in Figure R2 (right). The
46 height of the atmospheric boundary layer changed very little (less than 0.1 km) at noon.



47
48

49 **Fig. R2.** Retrieved aerosol extinction profile for a case study on 20 November,
50 2013. The black line represents the height of atmospheric boundary layer during
51 daytime (left). The atmospheric boundary layer height (BLK) was calculated from
52 China Meteorological Administration (CMA) meteorological observation data on 20
53 November, 2013 (right).

54

55 ***Comments and suggestions:***

56 *One other (and relatively minor) point on content: It would be helpful to add p*
57 *values for the correlations summarized in Table 3.*

58 **Responses and Revisions:**

59 Agreed and p values for the correlations have been added in Table R1 (Table 3 in
60 the revised manuscript). The p values for three events (#2, 4 and 5) are larger than 0.05,
61 the slopes are not significant correlation (at the 0.05 level). We have removed these
62 events (#2, 4 and 5) in Table R1 (Table 3).

63

64 Table R1. Coefficients of determination and slopes between GEM concentration
 65 and CO concentration during atmospheric mercury pollution events (* p<0.01).

E vent	Start Time (UTC + 8 hr)	End Time (UTC + 8 hr)	Du ration (h)	GE M (ng m ⁻³)	CO (ppbv)	GEM /CO (slop e, ng m ⁻³ ppbv ⁻¹)	R ²	p
1	2013/11/2 1 03:00	2013/11/22 02:00	23	8.37 ±2.42	4481.6± 717.3	0.001 8	0.2 9*	0.00 726
2	2013/12/0 3 20:00	2013/12/04 09:00	13	7.51 ±0.67	5270.0± 744.5	0.000 1	0.0 2*	0.651 15
3	2013/12/0 7 04:00	2013/12/09 04:00	48	9.21 ±1.16	5943.8± 1394.1	0.000 4	0.2 3*	5.82 259E-4
4	2013/12/1 9 09:00	2013/12/20 09:00	24	4.35 ±0.17	3907.6± 353.0	0.000 2	0.0 3*	0.74 582
5	2013/12/2 4 19:00	2013/12/25 15:00	20	5.58 ±0.94	4930.8± 919.7	0.001 2	0.0 1*	0.62 229
6	2014/01/1 7 22:00	2014/01/19 13:00	39	5.80 ±0.83	5746.3± 1626.9	0.000 3	0.2 8*	4.69 294E-4
7	2014/01/2 5 02:00	2014/01/25 22:00	20	6.03 ±0.50	8797.9± 2244.3	0.000 2	0.5 9*	6.91 209E-5
8	2014/03/1 6 05:00	2014/03/16 20:00	15	4.46 ±0.47	2261.7± 440.2	0.001 0	0.7 9*	4.03 625E-6
9	2014/03/1 7 06:00	2014/03/18 12:00	30	8.85 ±2.46	2697.1± 590.3	0.003 0	0.5 1*	6.98 676E-6
1 0	2014/05/2 1 00:00	2014/05/21 11:00	11	5.74 ±0.94	3676.7± 1690.0	0.005 0	0.7 9*	9.81 815E-5

66

67 **Comments and suggestions:**

68 *Although the English is quite good, it is not up to ACP standards. There are still*
 69 *many grammatical and punctuation errors and a few instances of poor word usage. I*
 70 *recommend that you ask a colleague who is a native English speaker to help you*
 71 *remedy this.*

72 **Responses and Revisions:**

73 Many thanks! We have thoroughly polished the English in the revised manuscript.

74

75

76

77

78

79

80

81

82

83

84

85

86

87

88

89

90

91

92

93

94

95

96

97

98

99

100

101

102

103

104

105

106

107

108 | **Speciated Atmospheric Mercury during Haze and Non-haze Days**
109 **in an Inland City in China**

110

111

112 Qianqian Hong^{1,3}, Zhouqing Xie^{1,2,3*}, Cheng Liu^{1,2,3*}, Feiyue Wang⁴, Pinhua Xie^{2,3},

113 Hui Kang¹, Jin Xu², Jiancheng Wang¹, Fengcheng Wu², Pengzhen He¹, Fusheng

114 Mou², Shidong Fan¹, Yunsheng Dong², Haicong Zhan¹, Xiawei Yu¹, Xiyuan Chi¹,

115 Jianguo Liu²

116

117

118 1. School of Earth and Space Sciences, University of Science and Technology of

119 China, Hefei, 230026, China

120 2. CAS Center for Excellence in Regional Atmospheric Environment & Institute of

121 Urban Environment of CAS, Xiamen, 361021, China

122 3. Key Lab of Environmental Optics and Technology, Anhui Institute of Optics and

123 Fine Mechanics, Chinese Academy of Sciences, Hefei, 230031, China

124 4. Centre for Earth Observation Science, and Department of Environment and

125 Geography, University of Manitoba, Winnipeg, MB R3T 2N2, Canada

126

127

128 Correspondence author:

129 zqxie@ustc.edu.cn (Z.Q.X.); chliu81@ustc.edu.cn (C.L.)

130

131

132 **Abstract.** Long-term continuous measurements of speciated atmospheric mercury
133 were conducted from July 2013 to June 2014 at Hefei, a mid-latitude inland city
134 in east central China that experiences frequent haze pollution. The mean
135 concentrations (\pm standard deviation) of gaseous elemental mercury (GEM), gaseous
136 oxidized mercury (GOM) and particle-bound mercury (PBM) were $3.95 \pm 1.93 \text{ ng m}^{-3}$,
137 $2.49 \pm 2.41 \text{ pg m}^{-3}$ and $23.3 \pm 90.8 \text{ pg m}^{-3}$, respectively, ~~on during~~ non-haze days, and
138 $4.74 \pm 1.62 \text{ ng m}^{-3}$, $4.32 \pm 8.36 \text{ pg m}^{-3}$ and $60.2 \pm 131.4 \text{ pg m}^{-3}$, respectively, ~~during~~
139 ~~on~~ haze days. Potential source contribution function (PSCF) analysis suggested that
140 ~~the~~ atmospheric mercury pollution ~~during on~~ haze days was caused primarily by local
141 ~~mercury~~ emissions, instead of via long-range ~~mercury~~ transport. The ~~disadvantageous~~
142 ~~diffusion poorer mixing conditions on during~~ haze days also favored the accumulation
143 of atmospheric mercury. Compared to GEM and GOM, PBM was ~~especially found to~~
144 ~~be more~~ sensitive to haze pollution. The mean PBM concentration ~~on during~~ haze days
145 was 2.5 times that ~~on during~~ non-haze days due to elevated concentrations of
146 particulate matter. ~~PBM also showed A remarkable clear~~ seasonal trend; ~~its in PBM~~
147 ~~was also observed with~~ concentration ~~was the highest in decreasing in the following~~
148 ~~order in response to the frequency of haze days:~~ autumn ~~and winter, decreased rapidly~~
149 ~~in , winter, spring,~~ and ~~was the lowest in~~ summer, ~~following the same order in the~~
150 ~~frequency of haze days in different seasons.~~ ~~On For~~ both non-haze and haze days,
151 GOM concentrations remained ~~at low relatively constant during at~~ night, but increased
152 rapidly ~~just before prior to sunrise, which . This GOM diurnal variation~~ could be due
153 to diurnal variation in air exchange between the boundary layer and free troposphere.
154 However, non-haze and haze days showed different trends ~~in between daytime GEM~~
155 and GOM ~~concentrations in the afternoon.~~ ~~On For~~ non-haze days, ~~GEM and GOM~~

156 ~~declined a synchronously decline on GEM and GOM through afternoon, probably due~~
157 ~~to the retreat of the free tropospheric air as the height of the might be related to the~~
158 ~~dilution effect from higher atmospheric boundary layer increases height. In contrast,~~
159 ~~on But for haze days, high-GOM and GEM concentrations showed opposite trends with~~
160 ~~the highest GOM and lowest GEM observed in the afternoon corresponded well with~~
161 ~~the lowest GEM concentration, along with the elevated boundary layer height,~~
162 ~~suggesting the occurrence of . This suggesting that except for FT transport, the~~
163 ~~contribution from photochemical oxidation could not be ruled out.~~ This is supported by
164 simple box-model calculations, which showed that oxidation of GEM to GOM does
165 occur and that the transport of free tropospheric GOM alone is not large enough to
166 account for the observed increase in daytime GOM. Our results further postulate that
167 NO₂ aggregation with the HgOH intermediate may be a potential mechanism for the
168 enhanced production of GOM during daytime.

169

170 1. Introduction

171 Mercury (Hg) is an environmental pollutant that has received much global
172 attention because of its toxicity and bioaccumulation ~~in via~~ the aquatic ~~food~~
173 ~~chain ecosystems~~. The most important transport pathway of mercury is via the
174 atmosphere (Schroeder and Munthe, 1998; Lindqvist and Rodhe, 1985).
175 Operationally, atmospheric mercury is commonly differentiated into
176 three forms: gaseous elemental mercury (GEM), gaseous oxidized mercury (GOM) and
177 particle-bound mercury (PBM). The sum of these three atmospheric speciated
178 mercury is defined as total atmospheric mercury (TAM=GEM+GOM+PBM), and the
179 sum of GEM and GOM is known as total gaseous mercury

180 (TGM=GEM+GOM)(Gustin and Jaffe, 2010;Gustin et al., 2015). Globally GEM is
181 ~~regarded as~~ the dominant form of atmospheric mercury, accounting for over 95% of
182 the total. GEM is stable in the troposphere with a long residence time (0.5–2 yr) and
183 can be transported at the regional to global scale(Schroeder and Munthe,
184 1998;Lindberg et al., 2007). GEM can be photochemically oxidized to GOM~~through~~
185 ~~photochemical processes, and which can be converted to further transformed to~~ PBM
186 upon adsorption on aerosol surfaces. Different from GEM, GOM and PBM can be
187 readily removed form the air by wet and dry depositionas a result oftheir high surface
188 affinity and water solubility (Lindqvist and Rodhe, 1985). Thus, ~~the~~ chemical
189 transformation between GEM, GOM and PBM will directly influence the atmospheric
190 lifetime of mercury.

191 As a result of ~~the~~ rapid industrial development and economic growth in of recent
192 decades, China hasbecome one of the major contributors to anthropogenic mercury
193 emissions to the environment(Wu et al., 2006;Pacyna et al., 2006;Pacyna et al.,
194 2010;Zhang et al., 2015b). Atmospheric mercury emissions from anthropogenic
195 sources in China have been estimated to be in the range of 500-700 tons/yr,
196 accounting for 25-30% of the total global anthropogenic mercury emissions(Streets et
197 al., 2005;Wu et al., 2006). Studies of Research into atmospheric mercury in China are
198 ~~is~~ therefore critical to the understanding of mercury cycling at both regional and
199 global scales. Long-term observation of atmospheric mercury has been conducted in
200 numerous different regions in China, including both urban and remote areas in China.
201 TGM concentrations ~~observed~~ in urban and industrial ~~areas regions of China~~ were
202 observed to be in the range of 2.7–35 ng m⁻³, higher than the values reported for
203 North America and Europe, and for the adjacent Asian countries such as Korea and

204 Japan (Weigelt et al., 2013;Fang et al., 2009;Marumoto et al., 2015). TGM and PBM
205 concentrations in remote areas of China were also found to be higher than those
206 observed in North America and Europe(Fu et al., 2008a;Fu et al., 2008b;Fu et al.,
207 2012;Liu et al., 2010).

208 In recent years, haze pollution has become a major concern in China due to its
209 impacts on visibility, air quality, and climate. It is well known that haze formation is
210 mainly dependent on the atmospheric relative humidity (RH) and the concentration of
211 airborne particles(Chen et al., 2003;Sun et al., 2013). Most studies on haze have
212 focused on the measurements of airborne particulate matter; few examined the
213 influence of haze on the chemistry of atmospheric mercury, especially PBM. ~~Here we~~
214 ~~report a one-year~~ ~~In this study, we conducted one year synchronous~~
215 ~~observations~~ real-time measurement of speciated atmospheric mercury in Hefei, an
216 inland city of China, which experiences frequent haze events. The comparison of
217 atmospheric mercury ~~in under~~ haze days and non-haze days ~~during the study period~~
218 allows us to examine the formation and deposition mechanisms of mercury, as well as
219 their temporal variations.

220

221 2. Methods

222 2.1 Study site

223 ~~Continuous measurements of speciated atmospheric mercury were undertaken in~~
224 Hefei (31°52' N, 117°17' E) ~~from July 2013 to June 2014.~~ Hefei is, the capital of Anhui
225 Province, ~~is located~~ in east central China, between the Changjiang (Yangtze River) and
226 the Huaihe (HuaiRiver). ~~The region is under Hefei has~~ a humid subtropical climate
227 with four distinct seasons: summer (June-August), ~~is considered to be summer,~~

228 | autumn (September-November), ~~to be autumn,~~ winter (December-February), and
229 | spring ~~(to be winter and March-May)~~ to be spring. The prevailing wind is southeasterly
230 | in summer and northwesterly in winter. Like many Chinese cities, Hefei has
231 | experienced rapid growth in the past 20 years, with a present-day. ~~The~~ total permanent
232 | population of is about 7.7 million. The city has also been witnessing an increasing
233 | frequency in haze pollution, especially in winter months.

234 | The monitoring site was located on the Science Island, a small peninsula on the
235 | Dongpu Reservoir in the northwestern outskirts of Hefei (Fig. 1). The sampling and
236 | analytical instruments were installed 1.5 m above the rooftop (~ 20 m above the
237 | ground) of the main building of Anhui Institute of Optics and Fine Mechanics. Further
238 | information about the monitoring site can be found in a previous study (Hu et al.,
239 | 2014). We chose this area as the monitoring site because it is ~~one of the cleanest areas~~
240 | ~~in Hefei~~, not adjacent to any direct pollution sources such as power plants, iron and
241 | steel works.

242 |

243 | **2.2 Measurements of speciated atmospheric mercury**

244 | From July 2013 to June 2014, simultaneous measurements of GEM, GOM and
245 | PBM speciated atmospheric mercury concentrations were ~~carried out performed~~ by an
246 | automated TekranTM mercury speciation system. The system consisted of a Model
247 | 2537B mercury analyzer combined with a Model 1130 GOM unit and a Model 1135
248 | PBM unit. The system was configured to measure GEM every 5 min., and GOM and
249 | PBM every 2 h.

250 | The details about the Tekran-based mercury speciation system can be found in
251 | Landis et al. (2002). In general, the automated measurement process can be

252 summarized as sample collection, thermal desorption and determination. During the
253 collection period, ambient air ~~was is~~ drawn to the system at a typical flow rate of 10
254 L/min. GOM and PBM in the air ~~are were~~ captured by a KCl-coated quartz annular
255 denuder in the 1130 unit and a quartz filter in the 1135 unit, respectively, whereas
256 GEM would pass through the denuder and filter and be quantified on the ~~Tekran~~
257 2537B analyzer by cold-vapor atomic fluorescence spectroscopy (CVAFS). After an
258 hour of sampling, the 1135 quartz filter and the 1130 denuder would be switched to the
259 thermal decomposition mode at 800°C and 500°C, respectively, with the resulting
260 Hg⁰ quantified by the 2537B unit in the next hour, while the 1135 and 1130 components
261 ~~are were~~ flushed with zero-mercury gas for the next sampling.

262 The instrument maintenance followed typical protocols used in similar
263 studies (Landis et al., 2002; Hu et al., 2014). The quartz annular denuder was recoated
264 every two weeks, the quartz filter was replaced once a month, and the Teflon filter (pore
265 size 0.2 μm) in the sample inlet was changed every two weeks. Automated
266 recalibration of the Tekran 2537B was performed every 25h using an internal mercury
267 permeation source. No calibration standards were available for GOM and PBM, but
268 the 1σ precision for GOM and PBM was about 15 % (Landis et al., 2002). The
269 detection limit in ambient air is about 0.5 ng m⁻³ for GEM (or TGM) at a resolution of
270 5 min, and 1 pg m⁻³ for GOM and PBM at a resolution of 2h (Gustin et al., 2015).
271 Although the Tekran-based mercury speciation technique has been widely used
272 around the world, recent studies have shown that the technique does not efficiently
273 collect all ~~GOM gaseous oxidized mercury~~ and thus may substantially underestimate
274 the concentration of reactive mercury (Huang et al., 2013; Gustin et al., 2013).

275 Therefore, the GOM values reported in this study should be considered as the lower
276 limit of ~~GOM gaseous oxidized mercury~~ in the air (Wang et al., 2014).

277

278 2.3 Ancillary ~~d~~Data

279 Standard meteorological measurements including air temperature, ~~air~~ pressure,
280 RH, wind direction and speed were observed with a 5-min resolution. CO was
281 measured by an automated infrared carbon monoxide analyzer (Model EC9830T,
282 Ecotech Inc., Australia), with a detection limit of 40 ppbv. O₃ was measured every 5
283 min by an ozone analyzer (Model EC9810B, Ecotech Inc., Australia); its detection
284 limit and accuracy ~~were~~ 0.5 ppbv and ~~0.001 ppm~~ 1 ppbv, respectively. NO₂ was
285 measured by a Multi axis differential optical absorption spectroscopy (MAX-DOAS)
286 instrument. The collected spectra were analyzed using the QDOAS spectral fitting
287 software suite developed at BIRA-IASB
288 (<http://uv-vis.aeronomie.be/software/QDOAS/>). PM_{2.5} (particulate matter ~~of~~ less than
289 2.5 µm in diameter) data ~~were~~ collected from ~~the~~ China air quality online analysis
290 platform (<http://www.aqistudy.cn/historydata/index.php>).

291

292 2.4 Potential Sources Contribution Function (PSCF) analysis

293 To identify ~~the~~ possible influence of long-range transport on the distribution of
294 atmospheric mercury in Hefei, we calculated backward trajectories of air masses
295 using the HYSPLIT (Hybrid Single-particle Lagrangian Integrated Trajectory) model
296 with the Global Data Assimilation System (GDAS 1°) developed by the National
297 Oceanic and Atmospheric Administration (NOAA)
298 (<http://www.ready.noaa.gov>) (Draxler and Hess, 1998). Considering ~~the~~ atmospheric

299 pollutants are mainly concentrated in ~~the~~ low altitudes during heavy pollution days,
300 the trajectory arrival heights were set at 500m to represent the boundary layer where
301 atmospheric pollutants were well mixed. In this study, 3-day back-trajectories were
302 generated hourly by ~~the~~ TrajStat, a software, ~~which employs including~~ HYSPLIT for
303 trajectory calculation (Wang et al., 2009).

304 The contributions of other ~~pollution~~ source regions to the atmospheric mercury at
305 Hefei ~~were~~ identified by the Potential Sources Contribution Function (PSCF)
306 analysis with ~~the~~ TrajStat ~~software~~. PSCF analysis has been shown to be useful in
307 spatially identifying ~~emission pollution~~ sources for pollutants with a long lifetime
308 such as elemental mercury and CO (Xu and Akhtar, 2010). The ~~study domain is~~
309 ~~divided into grid cells, and the~~ PSCF value ~~for each cell s for the grid cells in the~~
310 ~~study domain was~~ ~~ere~~ calculated by counting the trajectory segment endpoints that
311 terminate within ~~the~~ each cell. ~~The number of endpoints that fall in the ijth cell is~~
312 ~~designated as N_{ij}. The number of endpoints for the same cell corresponding to the~~
313 ~~atmospheric mercury concentration higher than an arbitrarily set criterion is defined to~~
314 ~~be M_{ij}. In this study, mean GEM concentration of 4 ng m⁻³ during the whole study~~
315 ~~period was used as the mercury pollution criterion.~~ The PSCF value for the ijth cell is
316 ~~then~~ defined as:

$$317 \text{PSCF}_{ij} = \frac{M_{ij}}{N_{ij}} W_{ij} \quad (2)$$

318 ~~where N_{ij} is the~~ ~~The number of endpoints that fall in the ijth cell, and M_{ij} is the~~ ~~is~~
319 ~~designated as N_{ij}. The number of endpoints in the~~ ~~for the same cell that has~~
320 ~~corresponding to the atmospheric~~ ~~a GEM mercury concentration higher than an~~
321 ~~arbitrarily set criterion; in this study the criterion was set to be 4 ng m⁻³ which is~~ ~~is~~
322 ~~defined to be M_{ij}. In this study, the mean GEM concentration of 4 ng m⁻³ during the~~

带格式的：缩进：首行缩进： 0 字

带格式的：下标

带格式的：下标

323 ~~wholeentire study period was used as the mercury pollution criterion.~~ W_{ij} is an
324 arbitrary weight function introduced to reduce the effect of small values of N_{ij} ~~to.~~ ~~The~~
325 ~~PSCF values were multiplied by W_{ij} to~~ better reflect the uncertainty in the values for
326 these cells (Polissar et al., 2001). The weight function reduces the PSCF values when
327 the total number of endpoints in a particular cell is less than 3 times the average value
328 of the end points per cell:

$$329 \quad W_{ij} = \begin{cases} 1.0 & N_{ij} \geq 3N_{ave} \\ 0.70 & 3N_{ave} > N_{ij} \geq 1.5N_{ave} \\ 0.40 & 1.5N_{ave} > N_{ij} \geq N_{ave} \\ 0.20 & N_{ave} > N_{ij} \end{cases} \quad (3)$$

330

331 3. Results

332 We intended to continuously monitor speciated atmospheric mercury
333 concentration_s over the course of a year; however, interruptions were inevitable due to
334 instrument maintenance, which resulted in loss of data for the following four periods:
335 (1) 25 September to 9 October 2013; (2) 5 ~~–~~–14 November 2013; (3) 9 ~~–~~–25 February
336 2014; and (4) 1 ~~–~~–14 April 2014. The rest of the data were grouped into haze days
337 and non-haze days according to the China Meteorological Administration's haze
338 standard (QX/T 113-2010). Haze days refer to the days when the atmospheric
339 visibility < 10 km and RH < 80% (Duan et al., 2016), and non-haze days refer to clear
340 days with the atmospheric visibility > 10 km. The visibility and RH information were
341 collected from the weather history data at the Luogang Airport of Hefei
342 (<http://www.wunderground.com/>). Throughout the study period of almost a year, a
343 total of 56 days were identified to be haze days, and 253 days to be non-haze days. All
344 the times reported herein are local time (UTC + 8 h).

345

346 3.1 Overall characteristics of speciated atmospheric mercury

347 The time series of GEM, GOM and PBM concentrations at the study site
348 throughout the study period are shown in Fig. 2, ~~and~~ their frequency distributions are
349 shown in Fig. S1 ~~(in the supporting information (SI)).~~ The mean (\pm standard deviation)
350 GEM, GOM and PBM concentrations during the ~~entire whole~~ study period were
351 $4.07 \pm 1.91 \text{ ng m}^{-3}$, $3.67 \pm 5.11 \text{ pg m}^{-3}$, and $30.0 \pm 100.3 \text{ pg m}^{-3}$, respectively (Table
352 1). ~~The~~ GEM concentrations in different seasons did not differ much, ~~with~~. ~~The~~ the
353 highest ~~GEM concentration occurred~~ in autumn ($4.51 \pm 2.10 \text{ ng m}^{-3}$) ~~and~~, ~~while~~ the
354 lowest in spring ($3.89 \pm 1.79 \text{ ng m}^{-3}$). GOM concentrations varied greatly, ~~during the~~
355 ~~study period~~ with much higher concentrations in autumn and the lowest in winter. A
356 similar seasonal variation in the GOM concentration was observed at a remote site in
357 Mt. Gongga of southwest China (Fu et al., 2008b). ~~PBM showed the highest degree of~~
358 ~~seasonal variability; The seasonal trend in PBM was also observed in Hefei with its~~
359 concentration decreased ~~ing~~ in the following order: autumn \approx winter > spring >
360 summer. The mean PBM concentration ~~in autumn and winter during the cold season~~
361 ~~were~~ about 20 times that in summer, similar to the findings from many previous
362 studies in China (Zhang et al., 2013; Fu et al., 2011; Fu et al., 2008b; Fang et al., 2001).

363 Comparisons of speciated atmospheric mercury concentrations with other urban
364 and rural areas in China and a few other countries are shown in Table 2. The mean
365 GEM concentration at Hefei is slightly higher than ~~those reported at in from~~ many
366 remote areas in China (Fu et al., 2008a; Fu et al., 2008b; Fu et al., 2012; Wan et al.,
367 2009a; Wan et al., 2009b; Zhang et al., 2015a), but is much lower than those ~~from in~~
368 urban areas of ~~heavily~~ industrial cities such as Guiyang and Changchun where large
369 point sources of mercury exist (e.g., non-ferrous metal smelting, coal-fired power

370 plants, and residential coal burning) (Feng et al., 2004;Fu et al., 2011;Fang et al.,
371 2004). Although Hefei is geographically close to Shanghai, a mega urban centre in
372 China, it is interesting to note that the TGM concentration of Shanghai is much lower
373 than that of Hefei. This may be due to the fact that Shanghai is a coastal city that is
374 influenced more by cleaner marine air masses (Friedli et al., 2011). Table 2 also
375 shows that the average concentration of GEM in Hefei ~~istypically more than~~
376 ~~doublesfold or two fold~~the typical values reported ~~that infrom~~ the urban and rural
377 areas in Europe and North America(Liu et al., 2010;Li et al., 2008;Brooks et al.,
378 2010).

379

380 3.2Speciated atmospheric mercury on during-non-haze days

381 ~~As shown in Table 1 and The frequency distribution of GEM, GOM and PBM for~~
382 ~~the non-haze period are shown in~~Fig.S1(in blue). ~~T~~he mean concentration of GEM
383 on non-haze days was $3.95 \pm 1.93 \text{ ng m}^{-3}$. Its distribution was characterized by large
384 ~~variations~~ ~~fluctuations~~ranging from 0.2 to 23.8 ng m^{-3} , although more than half of the
385 GEM values were in the narrow range ~~2~~ ~~4~~ ng m^{-3} . The mean concentration of
386 GOM on non-haze days was $2.49 \pm 2.41 \text{ pg m}^{-3}$ with a range of 0.5 ~~33.5~~ pg m^{-3} ,
387 although most of the values were in the range of 1-4 pg m^{-3} . High concentrations of
388 GOM (exceeding 10 pg m^{-3}) only accounted for 1.4% of the total data points. The
389 mean GOM concentration at ~~the~~-Hefei on these non-haze days site is much smaller
390 than ~~those~~at reported from other study sites in China (Table 2), but is comparable to
391 thevalues observed from many European and North American sites (Peterson et al.,
392 2012;Cheng et al., 2014;Ren et al., 2016). The mean PBM concentraion ~~at the Hefei~~
393 ~~site duringon~~ ~~the~~-non-haze days was $23.3 \pm 90.8 \text{ pg m}^{-3}$ with anexceptionally large

394 range of 0.5-1827 pg m^{-3} ; ~~The frequency distribution of PBM showed that~~ high
395 PBM concentrations (i.e., $> 50 \text{ pg m}^{-3}$) accounted for 6.4% of the total data points.
396 The PBM concentration under the non-haze condition in Hefei is generally ~~at a~~
397 similar ~~level~~ to values reported from the remote areas in western China, such as
398 Mt.Gongga, Mt.Waliguan and Shangri-Lai ~~in western China~~.

399 Diurnal variations of GEM, PBM and GOM concentrations ~~for on~~ non-haze days
400 are shown in Fig. 3. Both GEM and PBM concentrations exhibited similar ~~variations~~
401 patterns with elevated concentrations ~~at~~ during night. The GOM concentration
402 remained relatively constant ~~at~~ during night, but increased rapidly just before ~~prior to~~
403 sunrise and reached its peak value at $\sim 10:00$, followed by a synchronous decline with
404 GEM through afternoon (10:00-18:00).

405

406 3.3 Speciated atmospheric mercury on ~~during~~ haze days

407 Haze pollution mainly occurred in December and January at our monitoring site.
408 The four major haze pollution periods were identified in grey in Fig.2. The mean
409 concentrations of GEM, GOM and PBM ~~during on~~ these haze days were $4.74 \pm 1.62 \text{ ng}$
410 m^{-3} , $4.32 \pm 8.36 \text{ pg m}^{-3}$ and $60.2 \pm 131.4 \text{ pg m}^{-3}$, respectively (Table 1). The
411 frequency distributions of GEM, GOM and PBM on the haze days are shown in
412 Fig.S1 (in gray). ~~Comparison of GEM, GOM and PBM concentrations during haze~~
413 ~~and non haze days is shown in Fig.S2.~~ GEM, GOM and PBM concentrations show
414 significant differences between haze and non haze days ($p < 0.001$, t-test) (Fig. S2).
415 On average, the concentration of GEM on ~~in~~ haze days was 1.2 times that on ~~in~~
416 non-haze days. Similarly, the concentration of GOM on ~~in~~ haze days was about 1-1.7
417 times those on ~~in~~ non-haze days. The largest impact of haze pollution is however on

418 PBM, with the mean PBM concentration ~~on~~ haze days about 2.5 times that of
419 non-haze days. High concentrations of GOM (exceeding 10 pg m^{-3}) and PBM
420 concentrations (exceeding 50 pg m^{-3}) were also more frequently observed on haze
421 ~~days than in non-haze days~~, accounting for 5.9% and 25%, respectively, of the total
422 haze days.

423 ~~Diurnal variations of GEM, PBM and GOM concentrations for haze days are~~
424 ~~shown in~~ As shown in Fig. 3, on haze days the GEM concentration was s-were higher
425 at during night and lower, ~~decreased~~ during daytime. The PBM typically peaked just
426 before sunrise, with the lowest values occurred in the afternoon (14:00-16:00). The
427 opposite pattern was observed for GOM, which showed higher concentrations during
428 daytime than at during night. Although on both haze and non-haze days GOM showed
429 rapid increase just before Compared to non-haze days, the similar GOM trend was
430 found during night and early morning; GOM concentrations remained relatively
431 constant during night, but increased rapidly prior to sunrise, they exhibited different
432 trends during daytime. However, GOM also showed different trend from 10:00 to
433 18:00. On haze days, compared with non-haze days, the GOM peaked in the
434 afternoon when GEM was the lowest; corresponded well with the lowest GEM
435 value and the duration of the afternoon GOM peak was also lasted longer in the
436 afternoon for haze day on haze days.

437

438 4. Discussion

439 4.1 Influence of atmospheric mercury emission source

440 ~~In order to understand the mercury sources attribution, the PSCF model analysis~~
441 ~~was conducted by using the TrajStat software.~~ The With the year-long data seasonal

442 | mercury emission sources could be inferred from the PSCF analysis ~~with the~~
443 | ~~year-round data~~. Fig.4a showed the overall spatial contribution of mercury emission
444 | sources in China. As Hefei is located in east-central China, its atmospheric mercury
445 | concentration could be affected by both north and south emission sources, including
446 | those from the North China Plain (especially Shandong Province) and the neighboring
447 | provinces of Henan, Jiangsu, Jiangxi and Hubei. The total mercury emissions from
448 | Henan and Shandong provinces were estimated to be over 50 and 45 tons in 2010,
449 | respectively, making them two largest Hg emitters in China (Zhang et al., 2015b).
450 | Long-range transport could also impact ~~the~~ seasonal variations of atmospheric
451 | mercury in Hefei. As shown in Figure 4, in spring, the major contributors of
452 | atmospheric mercury to Hefei were from the southwestern region including the local
453 | area and ~~the~~ Jiangxi and Hunan ~~P~~rovinces. In summer, the main contributors were
454 | from north of Anhui, as well as Henan and Jiangxi ~~P~~rovinces, and even from the
455 | Pearl River Delta region in the far south. Since the number of haze days account only
456 | for 5.6% of the total days in spring and summer, we did not provide haze and non-haze
457 | PSCF results for spring and summer seasons. As autumn and winter are the prevalent
458 | seasons for haze pollution, one PSCF result for haze days and another for non-haze
459 | days are shown for autumn and winter, respectively. The statistically significant
460 | difference ($p < 0.001$) in the GEM concentration between non-haze days and haze days
461 | suggests that haze pollution could directly affect the concentration of elemental
462 | mercury. As shown in Figs. 4d and 4f, higher GEM concentration was mainly
463 | influenced by local emission sources ~~during on~~ haze days. ~~For On~~ non-haze days, the
464 | most important mercury sources to the monitoring site were not only the local
465 | emission sources, but also those from the neighboring region of Shandong, Henan and

466 Jiangxi ~~provinces~~ Provinces (see Figs. 4e and 4g). ~~In summary, Therefore,~~ the increase
467 ~~in the~~ GEM concentration ~~on during~~ haze days was mainly caused by local
468 emissions.

469 GEM and CO often share similar anthropogenic emission sources, such as
470 industrial coal combustion, domestic coal combustion, iron and steel production and
471 cement production (Wu et al., 2006; Wang et al., 2005). However, they also have their
472 ~~distinct own emission~~ sources. For instance, power plants and nonferrous metal
473 smelters emit mercury but hardly any CO₂; while automobiles contribute greatly to
474 ~~most of CO emission, they originates from vehicles which~~ are not a major emitter for
475 mercury. The correlation coefficients and slopes between GEM and CO
476 ~~concentration and CO concentration~~ during mercury pollution events are shown in
477 Table 3. These mercury pollution episodes were defined as when a period with the
478 hourly average GEM concentration was higher than seasonal average GEM
479 concentration for at least 10 consecutive and the duration of elevated hourly GEM
480 ~~concentration lasted for over 10~~ hours. ~~The Hg/CO slope and correlation between~~
481 ~~GEM and CO concentrations has been used to identify long-range transport episodes~~
482 ~~and local episodes in previous research (Jaffe et al., 2005; Weiss-Penzias et al.,~~
483 ~~2006; Kim et al., 2009).~~ These episodes could be classified into long-range transport
484 episodes or local episode by using the correlation coefficients (R^2) of linear regression
485 between Hg and CO: a significant positive correlation indicates for long-range
486 transport episodes and a poor correlation signals for local episodes (Kim et al.,
487 ~~2009) research (Jaffe et al., 2005; Weiss-Penzias et al., 2006; Kim et al., 2009). Using~~
488 this approach, we identified t three local episodes (events: 1-3) characterized by
489 ~~were found to have~~ poor correlations between GEM and CO concentrations

490 ($R^2:0.23-0.29$) ~~for local episodes, and while~~ four long-range transport episodes (events:
491 4-7) characterized by were found to have positive correlations between GEM and CO
492 concentrations ($R^2:0.51-0.79$) ~~for long-range transport episodes~~. These local episodes
493 tend to occur in autumn and winter. The slope of the trend line represents the Hg/CO
494 ratio, which could aid in the identification of specific emission sources. Emissions
495 from power plants typically have a higher Hg/CO ratio (Wu et al., 2006), whereas
496 residential coal and biomass burning combustion have a lower Hg/CO
497 ratio ($0.0013-0.0046 \text{ ng m}^{-3} \text{ ppbv}^{-1}$) due to incomplete combustion (Weiss-Penzias et al.,
498 2007). The Hg/CO ratio for vehicles is close to nearly zero (Zhang et al., 2013). The
499 Hg/CO ratios during the pollution episodes in from our study ~~for pollution episodes~~
500 ~~are in the range of~~ from of -0.0001 to $-0.0050 \text{ ng m}^{-3} \text{ ppbv}^{-1}$ suggesting mercury
501 emission in ~~In summary, the low GEM/CO ratio in Hefei during~~ autumn and winter in
502 Hefei could be might related to ~~the~~ local incomplete combustion sources, such as like
503 residential coal and biomass burning ~~combustion~~.

504

505 **4.2 Impacts of meteorological factors for atmospheric mercury on during haze** 506 **days**

507 Meteorological conditions, especially wind direction and speed, could also
508 impact ~~the~~ atmospheric mercury on during haze days. The wind rose for the
509 monitoring site during the study period is shown in Fig.5. Easterly and southeasterly
510 winds represented the prevailing wind directions at the study site. A wind rose
511 diagram of GEM concentrations above the 90th percentile value is shown in Fig.5B.
512 We found that 67% of the high GEM concentrations occurred at low wind speed
513 (below 1.5 m s^{-1}); however, wind speed below 1.5 m s^{-1} accounted for only 1.7% of

514 | ~~the total~~ study duration. High GOM and PBM concentrations appear not to be related
515 | to high wind speed (wind speed: 3-5 m s⁻¹); only 1.4% and 2.6% of the high GOM
516 | and PBM concentrations were observed under high wind-speed conditions,
517 | respectively (Figs. 5C and 5D). ~~The occurrence of~~ In general, most of the high
518 | atmospheric mercury levels ~~occurred in~~ the low wind speed conditions is to be
519 | expected, as. ~~This~~ this slow wind speed condition is not conducive to the spread and
520 | mixing of mercury especially on haze days, and thus favors mercury ~~the~~ accumulation
521 | in the air ~~of atmospheric mercury, especially during haze days~~. ~~This result is~~ further
522 | supports that atmospheric mercury on ~~during~~ haze days is mainly due to ~~affected~~ by
523 | local emissions.

524 | Both GEM and PBM concentrations exhibited diurnal ~~great~~ variations with
525 | elevated concentrations at ~~during~~ night or in early morning, regardless of the presence
526 | of haze. Such a diurnal variation ~~of GEM and PBM~~ could be related to changes in the
527 | height of the urban boundary layer. The diurnal trend of the boundary layer height
528 | (BLH or BLK) in Hefei is shown in Fig. S3, which is typically low in the morning
529 | and night, and high during the daytime on ~~for~~ both non-haze and haze days. Such
530 | diurnal changes in BLH in Hefei and nearby cities have also been observed in
531 | previous studies ~~The BLK daily variation result is also similar to the previous studies~~
532 | ~~which conducted in Hefei and surrounding cities~~ (Yuan et al., 2005; Mao et al., 2006).
533 | The maximum PBM concentration (observed at 6:00) was more than 4 times higher
534 | than the minimum value (observed at 16:00) on both ~~under~~ non-haze and haze days,
535 | with a ~~and about~~ 76% decrease from early morning to the afternoon ~~PBM were declined~~
536 | ~~during this period (6:00-16:00)~~. However, the reductions of PBM as a result of
537 | deposition during haze days was 62.7 pg m⁻³, which was about 2.4 times that in

538 non-haze days, suggesting that haze pollution could increase the removal of PBM.
539 Although PBM is not the major form of atmospheric mercury ~~emitted to the atmosphere~~,
540 it is crucial in atmospheric mercury transport and removal processes due to its short
541 atmospheric lifetime. As shown in Fig. 6, the highest PBM and PM_{2.5} concentrations
542 were observed in January, which is most likely due to a shallower boundary layer in
543 January than in other months. The co-variation in February is weaker, possibly due to
544 the loss of PBM data because of instrument maintenance ~~(see Section 2.3)~~. The PBM
545 concentration co-varied with the PM_{2.5} concentration, especially in January when all
546 the four PBM peak events were associated with increased PM_{2.5} concentrations (Fig.6c).
547 ~~These is~~ ~~result~~ ~~suggest~~ ~~indicates~~ ~~that~~ ~~the~~ ~~PM_{2.5} concentration~~ ~~may~~ ~~may~~ play an
548 important role in the formation of PBM. Thus, elevated PBM concentrations in autumn
549 and winter might be due to the combination of ~~the~~ poor mixing diffusion ~~conditions~~ ~~in~~
550 ~~cold months~~ and higher PM concentrations ~~pollution~~.

551

552 4.3 Enhancements in GOM and the potential GEM oxidation mechanism

553 Diurnal variations of GEM, GOM, O₃ and CO concentrations on during
554 non-haze and haze days are shown in Fig. 7. The weak correlation ($r=0.164$, $p<0.001$)
555 between GOM and CO suggests that the CO-producing, primary emission is not a
556 major source of GOM in the air. This is clearly shown in Fig. 7 (haze days), where the
557 peak value of GOM coincided with the lowest value of CO. As mentioned earlier, on
558 ~~For both non-haze and haze days, GOM concentrations remained relatively constant~~
559 ~~during night, but increased rapidly prior to sunrise. However, GOM showed different~~
560 ~~trends during through daytime-afternoon (10:00-18:00) between non-haze and haze~~
561 ~~days. On~~ ~~For~~ non-haze days, a synchronous decline was found between ~~on~~ GEM and

562 GOM in the afternoon, but opposite trend was observed between GEM and GOM for
563 on haze days. This ~~difference phenomenon~~ indicates that different GOM formation
564 mechanisms might be at work ~~on~~ during non-haze and haze days. Two processes can
565 affect the GOM concentrations in the boundary layer air. The first is the change ~~in~~ of
566 the atmospheric boundary layer height, which could ~~change the lead to the dilution of~~
567 ~~GOM and the transport of GOM-enriched~~ from the free tropospheric ~~e~~ (FT) air as the
568 ~~height of the boundary layer increases~~. Secondly, in situ photochemical oxidation of
569 ~~GEM could also would~~ increase the GOM concentration ~~of GOM~~ during daytime.
570 Various atmospheric oxidants are capable of oxidizing GEM to GOM, including
571 halogen radicals, ozone, hydroxyl radicals (OH), among others (Holmes et al.,
572 2010; Wang et al., 2014).

573 It is well established that FT contains higher GOM concentrations than in the
574 boundary layer (e.g., (Murphy et al., 2006; Lyman and Jaffe, 2012; Timonen et al.,
575 2013; Brooks et al., 2014; Shah et al., 2016)). ~~On~~ For both non-haze and haze days, it is
576 thus possible that the higher GOM concentrations observed prior to sunrise ~~are~~ due
577 to ~~enhanced admixing of~~ from the free tropospheric ~~air~~ as as the height of the
578 boundary layer increases ~~in~~ during the morning (see Fig. S3). ~~On~~ During non-haze
579 days, a synchronous decline ~~in~~ on GEM and GOM throughout afternoon (10:00-18:00)
580 might be related to the higher atmospheric boundary layer height during this
581 period. ~~The decline of GOM indicated that the influence of dilution might be greater~~
582 ~~than the transport of GOM from the FT.~~ However, ~~on~~ during haze days, opposite
583 variation was observed between GEM and GOM from 10:00-18:00, along with the
584 elevated boundary layer height. This suggests ~~ing~~ that ~~other than~~ ~~except~~ for FT
585 transport, photochemical oxidation of GEM might also play an important role in the

586 **enhancements of GOM.** To determine the relative importance of FT transport and in
587 situ photochemical oxidation, we examined the relationship between GOM and the
588 changes in the height of the atmospheric boundary layer and the odd oxygen ($O_x =$
589 $O_3 + NO_2$) concentrations. We used O_x because it is a more conserved tracer of the
590 extent of photochemical processes in the urban atmosphere (Herndon et al.,
591 2008; Wood et al., 2010), as O_3 reacts with NO emitted from automobiles to form NO_2 .
592 **Example results are shown in Fig. 8 for 20th November, 2013 (haze day). As can be**
593 **seen from the figure, GEM and GOM showed opposite trends in the afternoon**
594 **(12:00-16:00), along with higher O_x concentrations during this period. The height of**
595 **the atmospheric boundary layer changed very little (less than 0.1 km) over the same**
596 **period (see Fig. S4). This simple comparison suggests that the transport of FT GOM**
597 **might be limited and that at least some of the GOM were formed from in situ**
598 **oxidation of GEM.** Note that in our studies we could only calculate daytime O_x
599 concentrations, because NO_2 concentrations from MAX-DOAS were only available
600 during daytime.

601 We further investigated the mechanism of ~~the~~ GEM oxidation to GOM. Ozone
602 itself is not an efficient oxidant for GEM oxidation due to the low reaction rate (Hall,
603 1995; Holmes et al., 2010). Instead, halogen radicals (especially bromine atoms) and
604 OH halogen radicals, are believed to be the primary oxidants for GEM in the global
605 troposphere (Holmes et al., 2010). Unfortunately, we did not measure halogen
606 radicals in this study. OH radicals are known to be present in the early morning urban
607 boundary layer, primarily from the photolysis of HONO, which accumulates
608 during night (Kleffmann et al., 2005). Therefore, here we consider the oxidation of
609 GEM by OH radicals only. The formation of HgOH as an intermediate product of the

610 $\text{Hg}^0(\text{g}) + \text{OH}$ oxidation reactions has been proposed by Sommar et al., 2001, although
611 HgOH is highly unstable and could decompose back rapidly to Hg^0 and OH (Sommar
612 et al., 2001; Goodsite et al., 2004). It has been proposed that the presence of other
613 gases X ($X = \text{NO}_2, \text{HO}_2, \text{RO}, \text{RO}_2, \text{orNO}$) could assist the formation of Hg(II) by
614 forming $X\text{-HgOH}$, which outcompetes the decomposition of HgOH (Calvert and
615 Lindberg, 2005; Dibble et al., 2012; Wang et al., 2014). As an example, we calculated
616 the transformation between GEM and GOM under the influence of NO_2 , using the
617 reactions and rate constants shown in Table S1. As shown in Fig. S5, the production
618 rate of NO_2HgOH , $d[\text{NO}_2\text{HgOH}]/dt$, increased almost linearly with increasing NO_2
619 under low NO_2 concentrations, and eventually reached a steady state when the NO_2
620 concentration is high enough.

621 Based on the production rate of NO_2HgOH , we can estimate the production of
622 NO_2HgOH during the 1hr sampling period when GOM was captured by the
623 KCl-coated denuder in the Tekran 1130 unit. The production of NO_2HgOH and
624 $d[\text{NO}_2\text{HgOH}]/dt$ corresponding to different NO_2 concentrations is shown in Table 4.
625 With the increase of the NO_2 concentration, the contribution of the NO_2HgOH
626 production to GOM will increase. If the NO_2 concentration is within 100 ppbv (from
627 0 to 100 ppbv), the production of NO_2HgOH would be in the range of 0.058-4.81 pg
628 m^{-3} during the 1h sampling period. As illustrated in Table 4, the level of NO_2 observed
629 in our study is high enough to account for the ~~make~~ increase in the observed GOM
630 production. Our results thus support a recent study in the tropical equatorial Pacific
631 (Wang et al., 2014) that NO_2 aggregation with HgOH ~~provides~~ provides a possible
632 mechanism for to explain the enhanced production of GOM. If that is true, -and the
633 role of NO_2 would be expected to ~~might be~~ play an even more important role in the

634 urban air because of its higher concentration. More laboratory and modeling studies
635 on the mercury oxidation mechanism in the presence of NO₂ and other gases are thus
636 warranted.

637

638 5. Summary

639 Continuous measurements of speciated atmospheric mercury were conducted at
640 Hefei, a mid-latitude inland city in central China, from July 2013 to June 2014.
641 Measurements of other trace gases (e.g. CO, O₃, NO₂) and meteorological parameters
642 were employed to better understand the sources and oxidation pathways of
643 atmospheric mercury. The mean GEM, GOM and PBM concentrations during haze
644 days were $4.74 \pm 1.62 \text{ ng m}^{-3}$, $4.32 \pm 8.36 \text{ pg m}^{-3}$ and $60.2 \pm 131.4 \text{ pg m}^{-3}$, respectively.
645 Potential source contribution function (PSCF) analysis suggested that the local
646 mercury emission rather than long-range transport is the most important contributor of
647 atmospheric mercury pollution onduring haze days at our monitoring site. The low
648 GEM/CO ratio in Hefei could be indicative a result of local incomplete combustion
649 sources such as residential coal and biomass burning. Haze pollution has a more
650 profound impact on PBM than on GEM and GOM. PBM showed a remarkable
651 seasonal pattern, with higher concentrations in cold seasons and lower in warm
652 seasons. Elevated PBM concentrations might be due to both the high loadings of
653 particle matter and poorer mixing disadvantageous diffusion conditions onduring haze
654 days especially in cold months. Both GEM and PBM concentrations exhibited great
655 variations with elevated concentration during night. The diurnal variations of GEM
656 and PBM might be related to the boundary layer depth; a lower boundary layer depth
657 in the morning and night could elevate the mercury concentration.

658 | ~~Different from~~ ~~Unlike with~~ the diurnal variations of GEM and PBM, GOM
659 | concentration remained relatively constant ~~at during~~ night, and then increased rapidly
660 | prior to the sunrise. The enhancement of GOM during daytime could be due to both
661 | the transport of GOM-enriched free tropospheric~~ice~~air to the boundary layer and in situ
662 | oxidation of GEM in the boundary layer. Simple photochemical modeling supports
663 | the occurrence of daytime oxidation of GEM to GOM. Based on HgOH as an
664 | intermediate product, our calculations suggest that NO₂ aggregation with HgOH is a
665 | potential mechanism ~~for to explain~~ the enhanced production of GOM ~~in over~~ the
666 | inland urban air.

667

668

669 **Acknowledgements**

670 | This research was supported by grants from the National Basic Research Program of
671 | China (2013CB430000), the National Natural Science Foundation of China (Project
672 | Nos. 91544103,41575021) and the External Cooperation Program of BIC, CAS
673 | (Project No.211134KYSB20130012).

674

675 **References**

- 676 Brooks, S., Luke, W., Cohen, M., Kelly, P., Lefler, B., and Rappenglück, B.: Mercury
677 species measured atop the Moody Tower TRAMP site, Houston, Texas,
678 Atmospheric Environment, 44, 4045-4055, 2010.
- 679 Brooks, S., Ren, X., Cohen, M., Luke, W. T., Kelley, P., Artz, R., Hynes, A., Landing,
680 W., and Martos, B.: Airborne vertical profiling of mercury speciation near
681 Tullahoma, TN, USA, Atmosphere, 5, 557-574, 2014.
- 682 Calvert, J. G., and Lindberg, S. E.: Mechanisms of mercury removal by O₃ and OH in
683 the atmosphere, Atmospheric Environment, 39, 3355-3367, 2005.
- 684 Chen, L.-W. A., Chow, J. C., Doddridge, B. G., Dickerson, R. R., Ryan, W. F., and
685 Mueller, P. K.: Analysis of a summertime PM_{2.5} and haze episode in the
686 mid-Atlantic region, Journal of the Air & Waste Management Association, 53,
687 946-956, 2003.
- 688 Cheng, I., Zhang, L., Mao, H., Blanchard, P., Tordon, R., and Dalziel, J.: Seasonal and
689 diurnal patterns of speciated atmospheric mercury at a coastal-rural and a
690 coastal-urban site, Atmospheric Environment, 82, 193-205, 2014.
- 691 Dibble, T., Zelic, M., and Mao, H.: Thermodynamics of reactions of ClHg and BrHg
692 radicals with atmospherically abundant free radicals, Atmospheric Chemistry and
693 Physics, 12, 10271-10279, 2012.
- 694 Draxler, R. R., and Hess, G.: An overview of the HYSPLIT_4 modelling system for
695 trajectories, Australian meteorological magazine, 47, 295-308, 1998.
- 696 Duan, L., Xiu, G., Feng, L., Cheng, N., and Wang, C.: The mercury species and their
697 association with carbonaceous compositions, bromine and iodine in PM_{2.5} in
698 Shanghai, Chemosphere, 146, 263-271, 2016.

699 Fang, F., Wang, Q., and Li, J.: Atmospheric particulate mercury concentration and its
700 dry deposition flux in Changchun City, China, *Science of the total environment*, 281,
701 229-236, 2001.

702 Fang, F., Wang, Q., and Li, J.: Urban environmental mercury in Changchun, a
703 metropolitan city in Northeastern China: source, cycle, and fate, *Science of the Total*
704 *Environment*, 330, 159-170, 2004.

705 Fang, G.-C., Wu, Y.-S., and Chang, T.-H.: Comparison of atmospheric mercury (Hg)
706 among Korea, Japan, China and Taiwan during 2000-2008, *Journal of hazardous*
707 *materials*, 162, 607-615, 2009.

708 Feng, X., Shang, L., Wang, S., Tang, S., and Zheng, W.: Temporal variation of total
709 gaseous mercury in the air of Guiyang, China, *Journal of Geophysical Research:*
710 *Atmospheres* (1984-2012), 109, 2004.

711 Friedli, H., Arellano Jr, A., Geng, F., Cai, C., and Pan, L.: Measurements of
712 atmospheric mercury in Shanghai during September 2009, *Atmospheric Chemistry*
713 *and Physics*, 11, 3781-3788, 2011.

714 Fu, X., Feng, X., Zhu, W., Wang, S., and Lu, J.: Total gaseous mercury concentrations
715 in ambient air in the eastern slope of Mt. Gongga, South-Eastern fringe of the
716 Tibetan plateau, China, *Atmospheric Environment*, 42, 970-979, 2008a.

717 Fu, X., Feng, X., Zhu, W., Zheng, W., Wang, S., and Lu, J. Y.: Total particulate and
718 reactive gaseous mercury in ambient air on the eastern slope of the Mt. Gongga area,
719 China, *Applied Geochemistry*, 23, 408-418, 2008b.

720 Fu, X., Feng, X., Qiu, G., Shang, L., and Zhang, H.: Speciated atmospheric mercury
721 and its potential source in Guiyang, China, *Atmospheric Environment*, 45,
722 4205-4212, 2011.

723 Fu, X., Feng, X., Liang, P., Zhang, H., Ji, J., and Liu, P.: Temporal trend and sources of
724 speciated atmospheric mercury at Waliguan GAW station, Northwestern China,
725 Atmospheric Chemistry and Physics, 12, 1951-1964, 2012.

726 Goodsite, M. E., Plane, J., and Skov, H.: A theoretical study of the oxidation of Hg⁰ to
727 HgBr₂ in the troposphere, Environmental science & technology, 38, 1772-1776,
728 2004.

729 Gustin, M., and Jaffe, D.: Reducing the uncertainty in measurement and understanding
730 of mercury in the atmosphere, Environmental science & technology, 44, 2222-2227,
731 2010.

732 Gustin, M., Amos, H., Huang, J., Miller, M., and Heidecorn, K.: Measuring and
733 modeling mercury in the atmosphere: a critical review, Atmospheric Chemistry and
734 Physics, 15, 5697-5713, 2015.

735 Gustin, M. S., Huang, J., Miller, M. B., Peterson, C., Jaffe, D. A., Ambrose, J., Finley,
736 B. D., Lyman, S. N., Call, K., and Talbot, R.: Do we understand what the mercury
737 speciation instruments are actually measuring? Results of RAMIX, Environmental
738 science & technology, 47, 7295-7306, 2013.

739 Hall, B.: The gas phase oxidation of elemental mercury by ozone, in: Mercury as a
740 Global Pollutant, Springer, 301-315, 1995.

741 Herndon, S. C., Onasch, T. B., Wood, E. C., Kroll, J. H., Canagaratna, M. R., Jayne, J.
742 T., Zavala, M. A., Knighton, W. B., Mazzoleni, C., and Dubey, M. K.: Correlation
743 of secondary organic aerosol with odd oxygen in Mexico City, Geophysical
744 Research Letters, 35, 2008.

745 Holmes, C. D., Jacob, D. J., Corbitt, E. S., Mao, J., Yang, X., Talbot, R., and Slemr, F.:
746 Global atmospheric model for mercury including oxidation by bromine atoms,
747 Atmospheric Chemistry and Physics, 10, 12037-12057, 2010.

748 Hu, Q. H., Kang, H., Li, Z., Wang, Y. S., Ye, P. P., Zhang, L. L., Yu, J., Yu, X. W., Sun,
749 C., and Xie, Z. Q.: Characterization of atmospheric mercury at a suburban site of
750 central China from wintertime to springtime, Atmospheric Pollution Research, 5,
751 769-778, 2014.

752 Huang, J., Miller, M. B., Weiss-Penzias, P., and Gustin, M. S.: Comparison of gaseous
753 oxidized Hg measured by KCl-coated denuders, and nylon and cation exchange
754 membranes, Environmental science & technology, 47, 7307-7316, 2013.

755 Jaffe, D., Prestbo, E., Swartzendruber, P., Weiss-Penzias, P., Kato, S., Takami, A.,
756 Hatakeyama, S., and Kajii, Y.: Export of atmospheric mercury from Asia,
757 Atmospheric Environment, 39, 3029-3038, 2005.

758 Kim, S.-H., Han, Y.-J., Holsen, T. M., and Yi, S.-M.: Characteristics of atmospheric
759 speciated mercury concentrations (TGM, Hg (II) and Hg (p)) in Seoul, Korea,
760 Atmospheric Environment, 43, 3267-3274, 2009.

761 Kleffmann, J., Gavriloaiei, T., Hofzumahaus, A., Holland, F., Koppmann, R., Rupp, L.,
762 Schlosser, E., Siese, M., and Wahner, A.: Daytime formation of nitrous acid: A
763 major source of OH radicals in a forest, Geophysical Research Letters, 32, 2005.

764 Landis, M. S., Stevens, R. K., Schaedlich, F., and Prestbo, E. M.: Development and
765 characterization of an annular denuder methodology for the measurement of
766 divalent inorganic reactive gaseous mercury in ambient air, Environmental science
767 & technology, 36, 3000-3009, 2002.

768 Li, J., Sommar, J., Wängberg, I., Lindqvist, O., and Wei, S.-q.: Short-time variation of
769 mercury speciation in the urban of Göteborg during GÖTE-2005, *Atmospheric*
770 *Environment*, 42, 8382-8388, 2008.

771 Lindberg, S., Bullock, R., Ebinghaus, R., Engstrom, D., Feng, X., Fitzgerald, W.,
772 Pirrone, N., Prestbo, E., and Seigneur, C.: A synthesis of progress and uncertainties
773 in attributing the sources of mercury in deposition, *AMBIO: A Journal of the*
774 *Human Environment*, 36, 19-33, 2007.

775 Lindqvist, O., and Rodhe, H.: Atmospheric mercury-a review*, *Tellus B*, 37, 1985.

776 Liu, B., Keeler, G. J., Dvonch, J. T., Barres, J. A., Lynam, M. M., Marsik, F. J., and
777 Morgan, J. T.: Urban-rural differences in atmospheric mercury speciation,
778 *Atmospheric Environment*, 44, 2013-2023, 2010.

779 Lyman, S. N., and Jaffe, D. A.: Formation and fate of oxidized mercury in the upper
780 troposphere and lower stratosphere, *Nature Geoscience*, 5, 114-117, 2012.

781 Mao, M., Jiang, W., Wu, X., Qi, F., Yuan, R., Fang, H., Liu, D., and Zhou, J.: LIDAR
782 exploring of the UBL in downtown of the Nanjing City, *Acta Scientiae*
783 *Circumstantiae*, 26, 1723-1728, 2006.

784 Marumoto, K., Hayashi, M., and Takami, A.: Atmospheric mercury concentrations at
785 two sites in the Kyushu Islands, Japan, and evidence of long-range transport from
786 East Asia, *Atmospheric Environment*, 117, 147-155, 2015.

787 Murphy, D., Hudson, P., Thomson, D., Sheridan, P., and Wilson, J.: Observations of
788 mercury-containing aerosols, *Environmental science & technology*, 40, 3163-3167,
789 2006.

790 Pacyna, E. G., Pacyna, J. M., Steenhuisen, F., and Wilson, S.: Global anthropogenic
791 mercury emission inventory for 2000, *Atmospheric environment*, 40, 4048-4063,
792 2006.

793 Pacyna, E. G., Pacyna, J., Sundseth, K., Munthe, J., Kindbom, K., Wilson, S.,
794 Steenhuisen, F., and Maxson, P.: Global emission of mercury to the atmosphere
795 from anthropogenic sources in 2005 and projections to 2020, *Atmospheric*
796 *Environment*, 44, 2487-2499, 2010.

797 Peterson, C., Alishahi, M., and Gustin, M. S.: Testing the use of passive sampling
798 systems for understanding air mercury concentrations and dry deposition across
799 Florida, USA, *Science of the Total Environment*, 424, 297-307, 2012.

800 Polissar, A. V., Hopke, P. K., and Harris, J. M.: Source regions for atmospheric aerosol
801 measured at Barrow, Alaska, *Environmental science & technology*, 35, 4214-4226,
802 2001.

803 Ren, X., Luke, W. T., Kelley, P., Cohen, M. D., Artz, R., Olson, M. L., Schmeltz, D.,
804 Goldberg, D. L., Ring, A., and Mazzuca, G. M.: Atmospheric mercury
805 measurements at a suburban site in the Mid-Atlantic United States: Inter-annual,
806 seasonal and diurnal variations and source-receptor relationships, *Atmospheric*
807 *Environment*, 2016.

808 Schroeder, W. H., and Munthe, J.: Atmospheric mercury-an overview, *Atmospheric*
809 *Environment*, 32, 809-822, 1998.

810 Shah, V., Jaeglé, L., Gratz, L., Ambrose, J., Jaffe, D., Selin, N., Song, S., Campos, T.,
811 Flocke, F., and Reeves, M.: Origin of oxidized mercury in the summertime free
812 troposphere over the southeastern US, *Atmospheric Chemistry and Physics*, 16,
813 1511-1530, 2016.

814 Sommar, J., Gårdfeldt, K., Strömberg, D., and Feng, X.: A kinetic study of the
815 gas-phase reaction between the hydroxyl radical and atomic mercury, *Atmospheric*
816 *Environment*, 35, 3049-3054, 2001.

817 Streets, D. G., Hao, J., Wu, Y., Jiang, J., Chan, M., Tian, H., and Feng, X.:
818 Anthropogenic mercury emissions in China, *Atmospheric Environment*, 39,
819 7789-7806, 2005.

820 Sun, Z., Mu, Y., Liu, Y., and Shao, L.: A comparison study on airborne particles during
821 haze days and non-haze days in Beijing, *Science of the total environment*, 456, 1-8,
822 2013.

823 Timonen, H., Ambrose, J., and Jaffe, D.: Oxidation of elemental Hg in anthropogenic
824 and marine airmasses, *Atmospheric Chemistry and Physics*, 13, 2827-2836, 2013.

825 Wan, Q., Feng, X., Lu, J., Zheng, W., Song, X., Han, S., and Xu, H.: Atmospheric
826 mercury in Changbai Mountain area, northeastern China I. The seasonal distribution
827 pattern of total gaseous mercury and its potential sources, *Environmental research*,
828 109, 201-206, 2009a.

829 Wan, Q., Feng, X., Lu, J., Zheng, W., Song, X., Li, P., Han, S., and Xu, H.:
830 Atmospheric mercury in Changbai Mountain area, northeastern China II. The
831 distribution of reactive gaseous mercury and particulate mercury and mercury
832 deposition fluxes, *Environmental research*, 109, 721-727, 2009b.

833 Wang, F., Saiz-Lopez, A., Mahajan, A., Martín, J. G., Armstrong, D., Lemes, M., Hay,
834 T., and Prados-Roman, C.: Enhanced production of oxidised mercury over the
835 tropical Pacific Ocean: a key missing oxidation pathway, *Atmospheric Chemistry*
836 *and Physics*, 14, 1323, 2014.

837 Wang, L., Zhang, Q., Hao, J., and He, K.: Anthropogenic CO emission inventory of
838 Mainland China, *Acta Scientiae Circumstantiae*, 25, 1580-1585, 2005.

839 Wang, Y., Zhang, X., and Draxler, R. R.: TrajStat: GIS-based software that uses
840 various trajectory statistical analysis methods to identify potential sources from
841 long-term air pollution measurement data, *Environmental Modelling & Software*,
842 24, 938-939, 2009.

843 Weigelt, A., Temme, C., Bieber, E., Schwerin, A., Schuetze, M., Ebinghaus, R., and
844 Kock, H. H.: Measurements of atmospheric mercury species at a German rural
845 background site from 2009 to 2011—methods and results, *Environmental Chemistry*,
846 10, 102-110, 2013.

847 Weiss-Penzias, P., Jaffe, D. A., Swartzendruber, P., Dennison, J. B., Chand, D., Hafner,
848 W., and Prestbo, E.: Observations of Asian air pollution in the free troposphere at
849 Mount Bachelor Observatory during the spring of 2004, *Journal of Geophysical*
850 *Research: Atmospheres*, 111, 2006.

851 Weiss-Penzias, P., Jaffe, D., Swartzendruber, P., Hafner, W., Chand, D., and Prestbo,
852 E.: Quantifying Asian and biomass burning sources of mercury using the Hg/CO
853 ratio in pollution plumes observed at the Mount Bachelor Observatory, *Atmospheric*
854 *Environment*, 41, 4366-4379, 2007.

855 Wood, E., Canagaratna, M., Herndon, S., Onasch, T., Kolb, C., Worsnop, D., Kroll, J.,
856 Knighton, W., Seila, R., and Zavala, M.: Investigation of the correlation between
857 odd oxygen and secondary organic aerosol in Mexico City and Houston,
858 *Atmospheric Chemistry and Physics*, 10, 8947-8968, 2010.

859 Wu, Y., Wang, S., Streets, D. G., Hao, J., Chan, M., and Jiang, J.: Trends in
860 anthropogenic mercury emissions in China from 1995 to 2003, *Environmental*
861 *science & technology*, 40, 5312-5318, 2006.

862 Xu, X., and Akhtar, U.: Identification of potential regional sources of atmospheric total
863 gaseous mercury in Windsor, Ontario, Canada using hybrid receptor modeling,
864 *Atmospheric Chemistry and Physics*, 10, 7073-7083, 2010.

865 Yuan, S., Xin, Y., and Zhou, J.: Lidar Observations of the Lower Atmosphere in Hefei,
866 *Chinese Journal of Atmospheric Sciences*, 29, 387-395, 2005.

867 Zhang, H., Fu, X., Lin, C., Wang, X., and Feng, X.: Observation and analysis of
868 speciated atmospheric mercury in Shangri-La, Tibetan Plateau, China, *Atmospheric*
869 *Chemistry and Physics*, 15, 653-665, 2015a.

870 Zhang, L., Wang, S., Wang, L., and Hao, J.: Atmospheric mercury concentration and
871 chemical speciation at a rural site in Beijing, China: implications of mercury
872 emission sources, *Atmospheric Chemistry and Physics*, 13, 10505-10516, 2013.

873 Zhang, L., Wang, S., Wang, L., Wu, Y., Duan, L., Wu, Q., Wang, F., Yang, M., Yang,
874 H., and Hao, J.: Updated Emission Inventories for Speciated Atmospheric Mercury
875 from Anthropogenic Sources in China, *Environmental science & technology*, 49,
876 3185-3194, 2015b.

877

878

879

880 **Table 1. Summary of GEM, GOM and PBM concentrations measured in Hefei**
881 **from July 2013 to June 2014.**

882

	GEM (ng m ⁻³)			GOM (pg m ⁻³)			PBM (pg m ⁻³)		
	Mean ± σ	Range	N	Mean ± σ	Range	N	Mean ± σ	Range	N
Spring	3.89 ± 1.79	0.2-21.3	7890	4.49 ± 4.22	0.5-69.8	526	8.34 ± 8.97	1.6-130.1	542
Summer	4.08 ± 1.99	0.3-22.9	6050	3.66 ± 4.39	0.5-45.2	511	3.61 ± 4.38	0.5-41.9	570
Autumn	4.51 ± 2.10	0.4-23.8	3632	5.65 ± 8.93	0.5-78.9	274	59.9 ± 153.5	0.5-1615	339
Winter	4.05 ± 1.81	0.9-12.2	6381	2.59 ± 2.58	0.5-9.5	541	56.1 ± 134.9	0.5-1827	639
Total	4.07 ± 1.91	0.2-23.8	23953	3.67 ± 5.11	0.5-78.9	1852	30.02 ± 100.3	0.5-1827	2090
Non-haze	3.95 ± 1.93	0.2-23.8	20345	2.49 ± 2.41	0.5-33.5	1508	23.3 ± 90.76	0.5-1827	1708
Haze	4.74 ± 1.62	2.1-16.5	3608	4.32 ± 8.36	0.5-78.9	344	60.2 ± 131.4	1.6-1615	382

883

884

885 **Table 2. Speciated atmospheric mercury concentrations in Hefei and other urban**
 886 **and rural areas.**

887

888

Location	Classification	Time	TGM (ng m ⁻³)	GEM (ng m ⁻³)	GOM (pg m ⁻³)	PBM (pg m ⁻³)	Reference
Hefei	Suburb	Jul 2013-Jun 2014	4.1	4.07	3.67	30	This study
Hefei	Suburb	Feb-May 2009	2.53	-	-	-	Hu et al. (2014)
Beijing	Rural	Dec2008-Nov2009	3.23	3.22	10.1	98.2	Zhang et al. (2013)
Shanghai	Urban	Aug-Sep 2009	2.7	-	-	-	Friedli et al. (2011)
Nanjing	Urban	Jan-Dec 2011	7.9	-	-	-	Zhu et al. (2012)
Guiyang	Urban	Nov 2001-Nov 2002	8.4	-	-	-	Fenget al. (2004)
Guiyang	Urban	Aug-Dec 2009	-	9.72	35.7	368	Fu et al. (2011)
Changchun	Urban	Jul 1999-Jan 2000	18.4	-	-	276	Fang et al. (2004)
Changchun	Suburb	Jul 1999-Jan 2000	11.7	-	-	109	Fang et al. (2004)
Mt.Changbai	Remote	Aug2005-Jul 2006	3.58	-	65	77	Wan et al. (2009a,b)
Mt.Gongga	Remote	May 2005-July 2006	3.98	-	6.2	30.7	Fu et al. (2008a,b)
Mt.Waliguan	Remote	Sep 2007-Aug 2008	1.98	-	7.4	19.4	Fu et al. (2012a)
Mt.Leigong	Remote	May2008-May 2009	2.8	-	-	-	Fu et al. (2010)
Shangri-La	Remote	Nov 2009-Nov 2010	2.55	-	8.22	38.82	Zhang (2015)
Detroit, USA	Urban	Jan-Dec 2004	-	2.5	15.5	18.1	Liu et al. (2010)
Dexter, USA	Rural	Jan-Dec 2004	-	1.6	3.8	6.1	Liu et al. (2010)
Houston, USA	Urban	Aug-Oct 2006	-	1.66	6.9	2.5	Brooks et al. (2010)
Florida, USA	Urban	Jul 2009-Jul 2010	-	1.3	3	2	Peterson et al. (2012)
Maryland, USA	suburb	2007-2015	-	1.41	4.6	8.6	Ren et al. (2016)
Göteborg,Sweden	Urban	Feb-Mar 2005	-	1.96	2.53	12.5	Li et al. (2008)
Nova Scotia,Canada	Urban	Jan 2010- Dec 2011	-	1.67	2.07	2.32	Cheng et al.(2014)
Northern Hemisphere background value				1.5-1.7			Lindberg et al. (2007)

889

890 **Table 3. Coefficients of determination and slopes between GEM and CO**
891 **concentrations and CO concentration during atmospheric mercury pollution**
892 **episodesvents (*p<0.01).**

893

Event	Start Time (UTC + 8 hr)	End Time (UTC + 8 hr)	Duration (h)	GEM (ng m ⁻³)	CO (ppbv)	GEM/CO (slope, ng m ⁻³ ppbv ⁻¹)	R ²
1	2013/11/21 03:00	2013/11/22 02:00	23	8.37±2.42	4481.6±717.3	0.0018	0.29*
2	2013/12/07 04:00	2013/12/09 04:00	48	9.21±1.16	5943.8±1394.1	0.0004	0.23*
3	2014/01/17 22:00	2014/01/19 13:00	39	5.80±0.83	5746.3±1626.9	0.0003	0.28*
4	2014/01/25 02:00	2014/01/25 22:00	20	6.03±0.50	8797.9±2244.3	0.0002	0.59*
5	2014/03/16 05:00	2014/03/16 20:00	15	4.46±0.47	2261.7±440.2	0.0010	0.79*
6	2014/03/17 06:00	2014/03/18 12:00	30	8.85±2.46	2697.1±590.3	0.0030	0.51*
7	2014/05/21 00:00	2014/05/21 11:00	11	5.74±0.94	3676.7±1690.0	0.0050	0.79*

894 Notes: these episodes were identified when using the following criteria: (a) the
895 duration of elevated GEM concentration lasted for >10h; (b) the selected the hourly
896 average GEM concentration was higher than the seasonal average GEM concentration:
897 for more than 10 consecutive hours

898

899

900

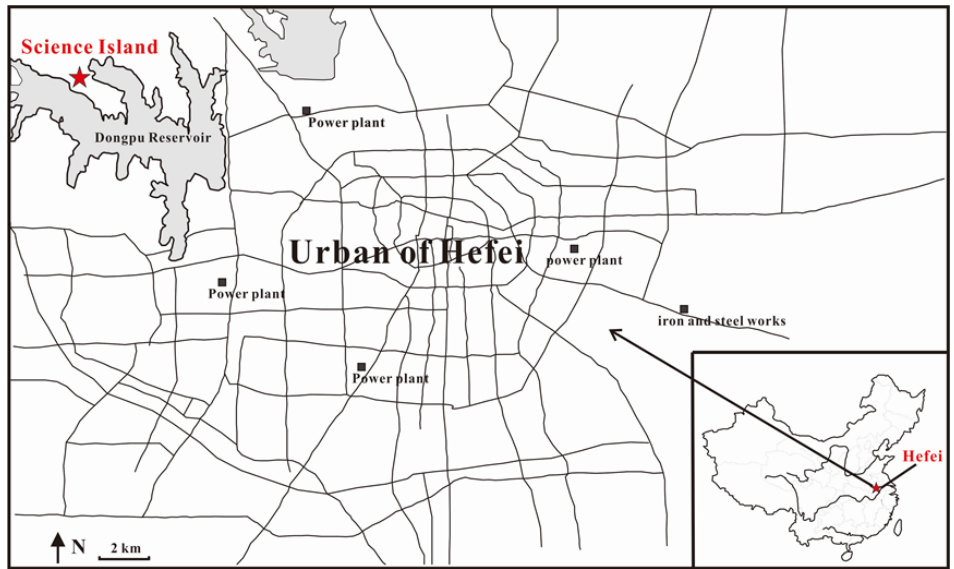
901 **Table 4. The production of NO₂HgOH and d[NO₂HgOH]/dt at different NO₂**

902 **concentrations**

903

NO ₂ (ppbv)	10	20	30	40	50	60	70	80	90	100
d(NO ₂ HgOH)/dt (molecule cm ⁻³ s ⁻¹)	0.36	0.71	1.04	1.37	1.68	1.99	2.28	2.56	2.83	3.10
NO ₂ HgOH (pg m ⁻³ , 1hr)	0.56	1.10	1.63	2.13	2.61	3.08	3.54	3.97	4.40	4.81

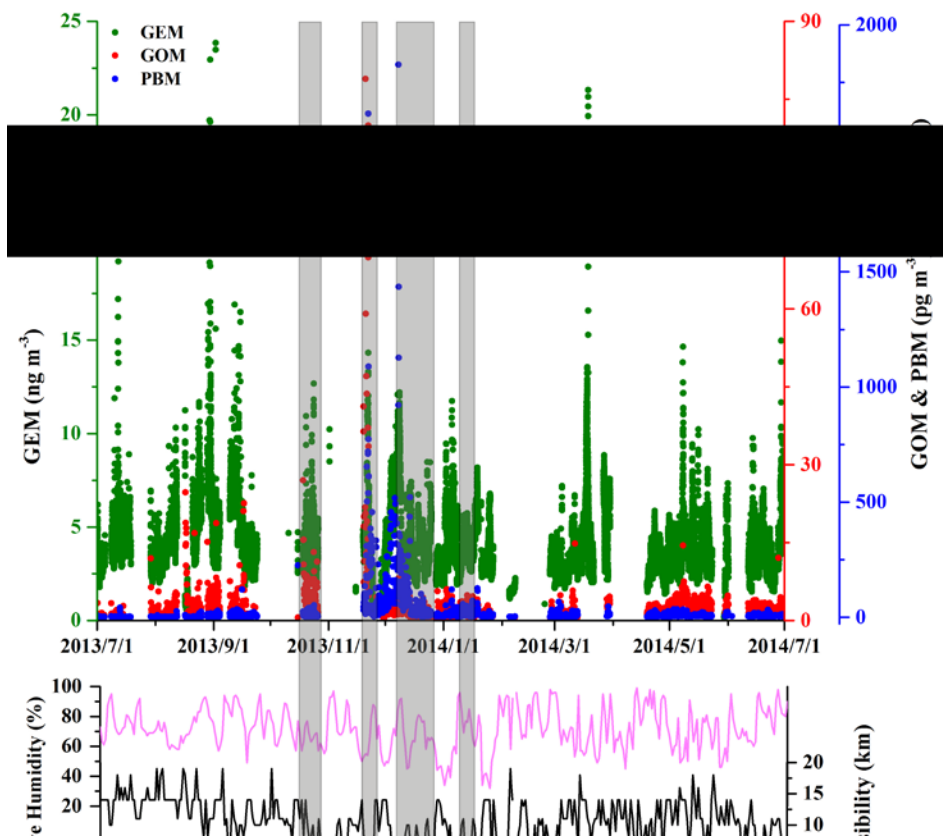
904
905
906



907
908
909
910

Fig. 1. Location of the study site in Hefei, China.

911
912



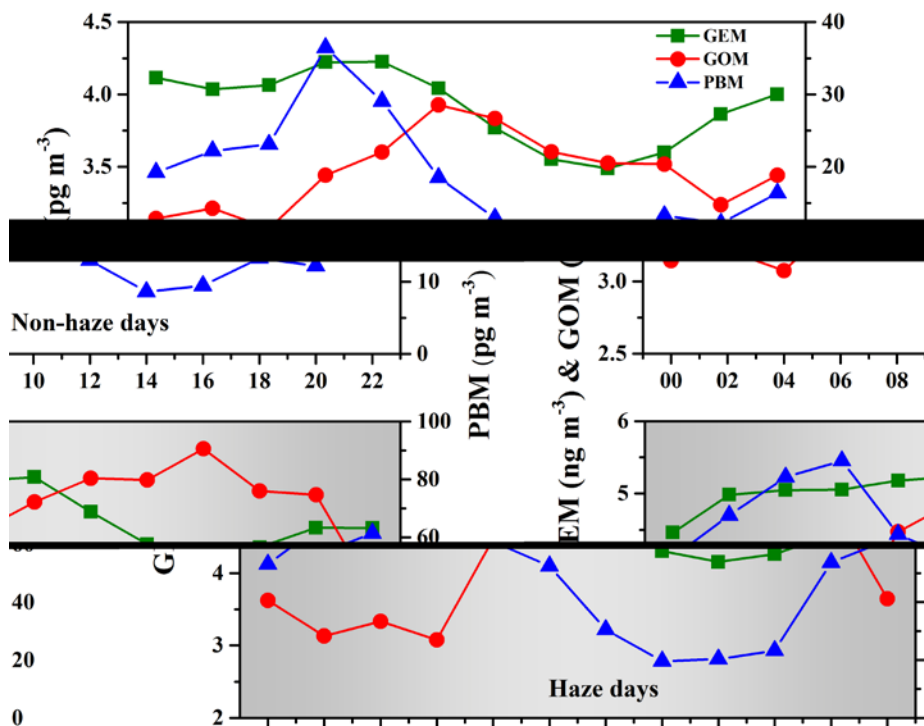
913
914

915 **Fig. 2.** Time series of GEM, GOM and PBM concentrations, along with visibility,
916 relative humidity, at the monitoring site in Hefei from July 2013 to June 2014. The
917 GEM data were at a 5-min resolution, and the GOM and PBM data were two-hour
918 averages. The gray columns show the major haze pollution episodes occurred during
919 the study period.

920
921
922
923

924

925



926

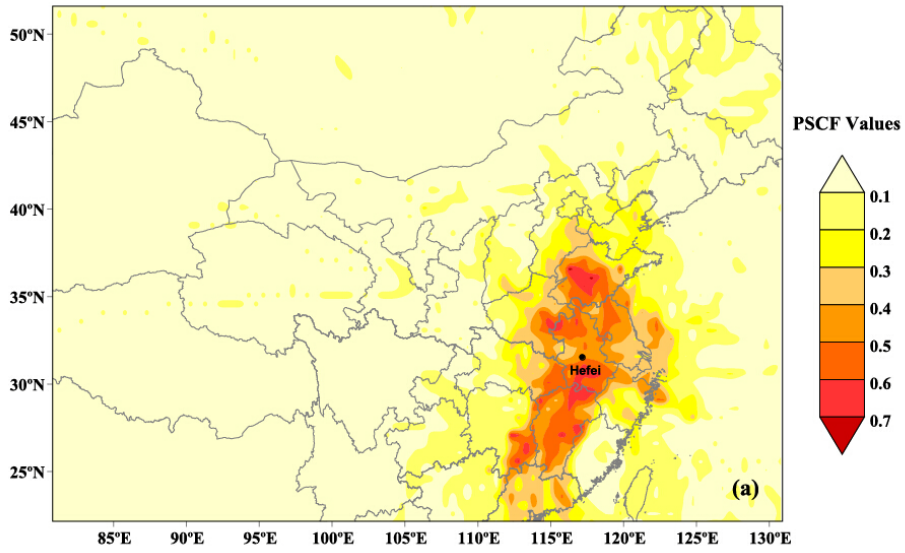
927

928 | **Fig. 3.** Diurnal trends of GEM, GOM and PBM concentrations in Hefei on during

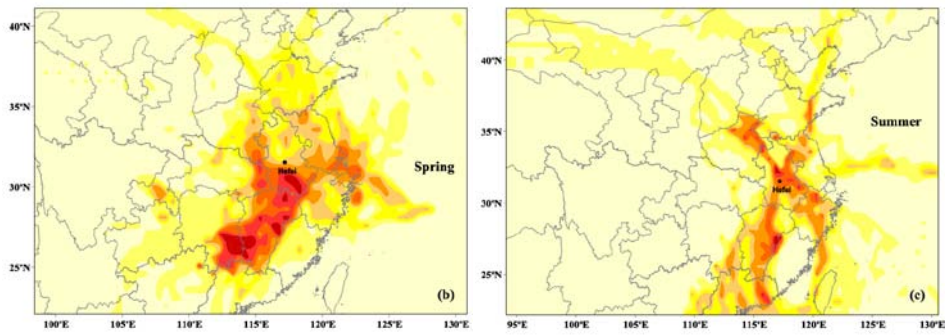
929 non-haze and haze days (Local time = UTC + 8 hr). The data were two-hour averages.

930

931
932

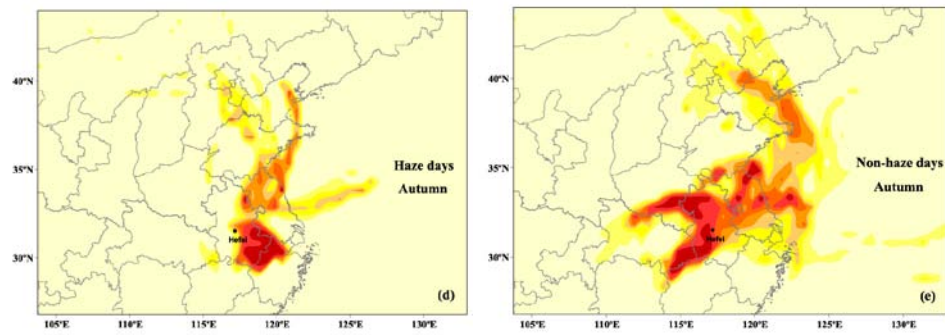


933



934

935

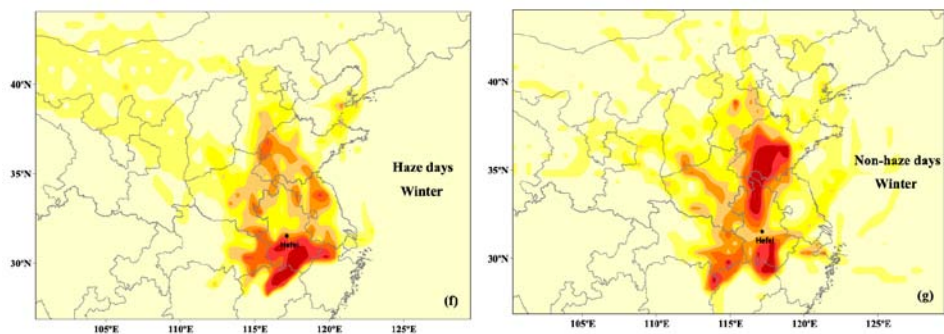


936

937

938

939



940

941

942 | **Fig. 4.** Likely emission source areas of GEM identified ~~simulated~~ by PSCF analysis.

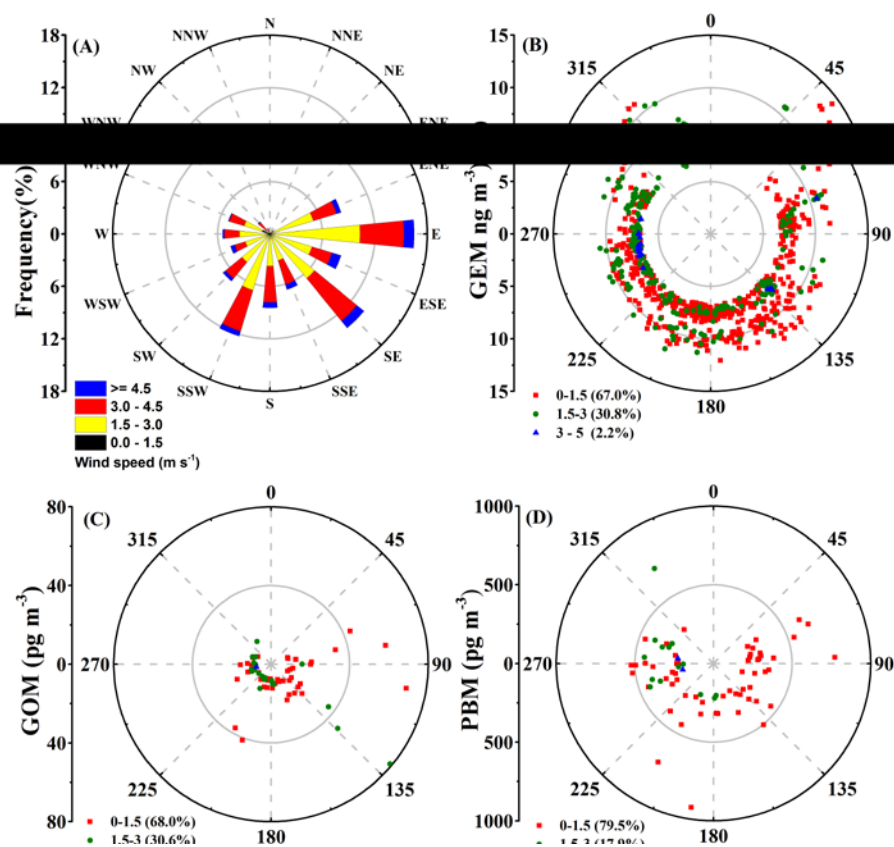
943 (a) overall (from July 2013 to June 2014), (b) spring, (c) summer, (d) haze days in

944 autumn, (e) non-haze days in autumn, (f) haze days in winter, (g) non-haze days in

945 winter.

946

947
948
949



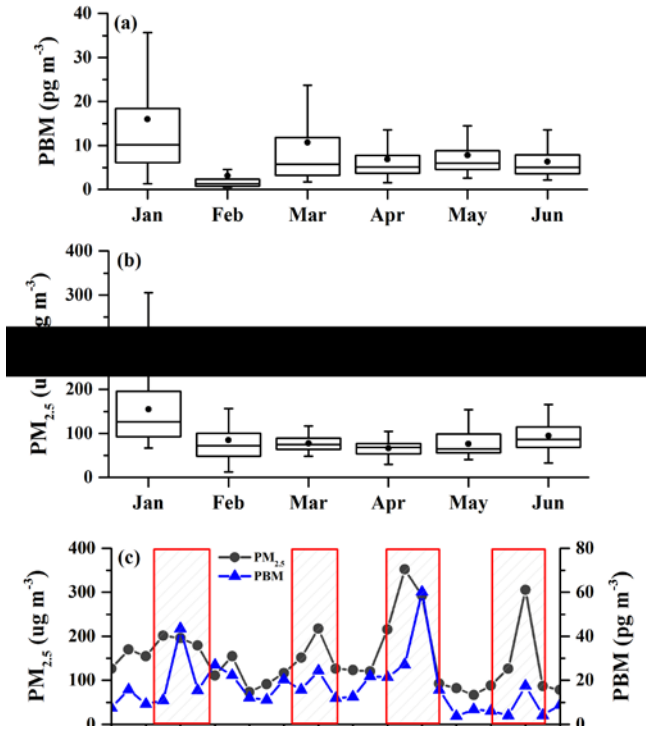
950
951
952

953 **Fig. 5.** Wind direction and speed at the monitoring station Science Island
954 Meteorological Station during the study period. (A) the wind rose for the entire whole
955 study period; (B), (C) and (D) are the wind rose diagrams for GEM, GOM and PBM
956 concentrations above the 90th percentile values, respectively.

957
958
959
960

961

962



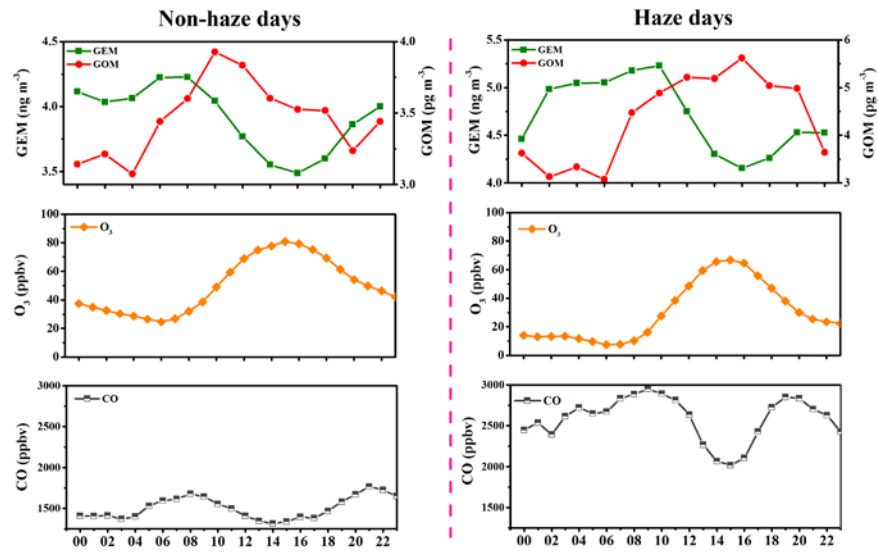
963

964 **Fig. 6.** Monthly variation of (a) PBM and (b) $\text{PM}_{2.5}$ concentrations from January to

965 June, 2014, (c) average daily $\text{PM}_{2.5}$ and PBM concentrations in January, 2014.

966

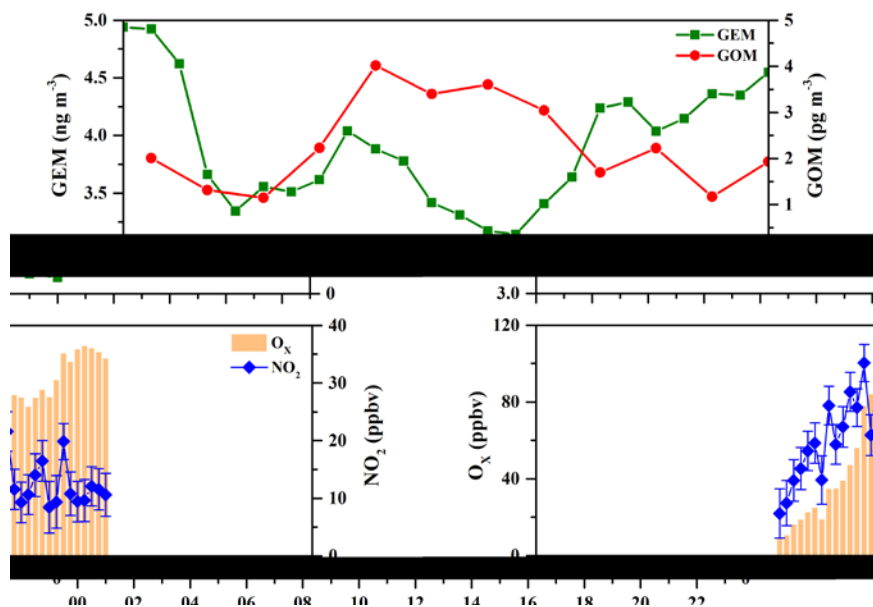
967
968



969
970
971
972
973

Fig. 7. Diurnal variations of GEM, GOM, O₃ and CO concentrations on during non-haze and haze days.

974



975

976 **Fig. 8.** A case study of diurnal variations of GEM, GOM, O_x, and NO₂ at Hefei (20th
977 November, 2013). The top panel shows the hourly averaged GEM and GOM
978 concentrations, and the bottom panel shows the O_x (O_x = NO₂ + O₃) and the NO₂
979 concentrations. The error bars for NO₂ refer to the NO₂ standard errors.

980